Comparison of the Utilization of Brushless DC Servomotors with Different Rotor Length by 3D - Finite Element Analysis

G. Henneberger, S. Domack and J. Berndt
Institute of Electrical Machines, University of Technology Aachen,
Schinkelstrasse 4, 52056 Aachen, F.R.Germany

Abstract –**This paper describes the influence of the stator end winding coils on two different asymmetrical rotor types with short motorlength. A current control method is applied to use the reluctance of the rotor and to reach minimal current consumption. Due to the saturation, 3D- finite elements field calculations are compared with the 2D- finite element field calculation. Different rotor lengths are taken into account and a difference of rotor length to stator length is examined. To regard the effect of saturation, different current levels are calculated.**

I. Introduction

Permanent magnet excited machines are applied in servodrives for machine tools and robotics. Excellent dynamic behavior, high position precision and low torque ripples are requested. To reduce the motor volume, high energy rare earth magnets (SmCo) are used. A current control method [1] is applied to reach minimal current consumption and to economize the expensive magnet material. Therefore an asymmetrical rotor geometry is used with $X_q > X_d$. For some robot applications short motor lengths are desirable. Thus the end winding leakage is an essential influence factor for the motor length. At high current levels the output torque is not as high as calculated, even if saturation is considered.

II. Current Control Method and Rotor Design

For the conventional servomotor the stator currents are controlled with a pole position sensor, so that the stator m.m.f and the rotor field have a constant phase angle of 90° between them. This means the armature current has only a quadrature component. The reactances in the quadrature and direct axes have the same value, because the whole rotor surface is covered with magnets.

If we construct a motor with a greater quadrature reactance X_q than the direct reactance X_d , and increase the angle between the stator m.m.f. and the rotor field, it is possible to increase the output torque. The rotor reluctance in combination with a negative current component provides additional torque. Fig. 1 shows the phasor diagram.

Manuscript recieved November 1, 1993.

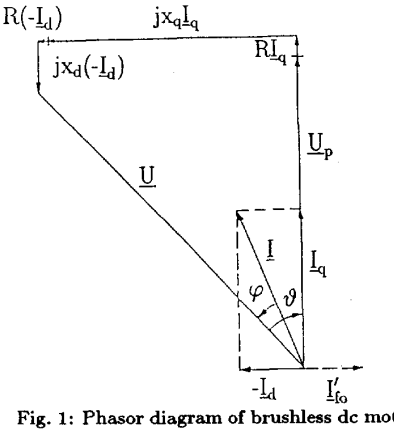

Fig. 1: Phasor diagram of brushless dc motor.

The general equations for torque and current with an asymmetrical rotor design are as follows:

$$I_d = I \cdot \sin(\psi) \quad , \tag{1}$$

$$I_q = I \cdot \cos(\psi) \quad , \tag{2}$$

$$M = \frac{3p}{\omega}(U_{P0} - I_d(X_q - X_d))I_q \quad . \tag{3}$$

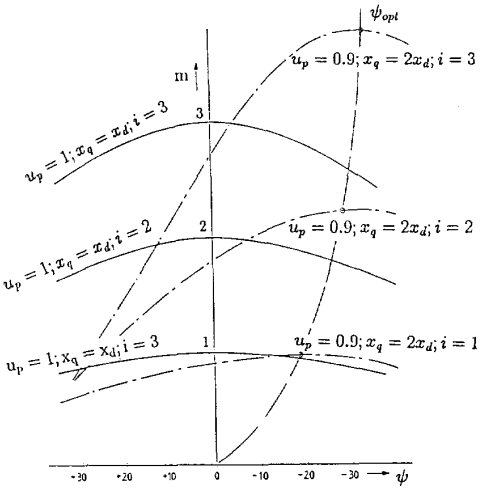

Fig. 2: Rated torque as a function of the load angle ψ for symmetric and asymmetric rotor design at different current levels.

0018-9464/94$4.00 © 1994 IEEE

For the calculation and comparison of the symmetric and asymmetric motor, the torque equation can be expressed with the load angle ψ. Fig. 2 shows the output torque as a function of the load angle ψ and the current i as a parameter. The per unit value of the induced e.m.f. for the asymmetric rotor is set to 0.9 in order to save magnet material. The value for X_q is assumed to be $2X_d$. With a pure quadrature current component the asymmetric motor therefore reaches only 90% of the torque output in comparison to the symmetric motor. This reduction of torque can be compensated for by a negative current component at low current values. At high current values a remarkable torque increase can be obtained [1].

The desired inequality of reactances X_q and X_d can be obtained in different ways. A simple method to get an asymmetrical rotor is by changing the outside magnet pieces of the pole pitch into iron (Fig. 4). The second method is the rotor with interior radial magnets (Fig. 5).

III. Experimental Effects

The rotor geometry is asymmetrical with $X_q > X_d$. The measured inductances give a reactance ratio of $\frac{X_q}{X_d}$=1.85. The three phase stator windings are fed sinusodially and the induced air gap flux density is rectangular (mixed mode). This mode has in connection with a two layer stator winding the best machine utilisation [1]. The rotor design with outside iron pieces like in Fig. 4 was constructed with short rotor (16mm) length in respect to stator windings (68mm).

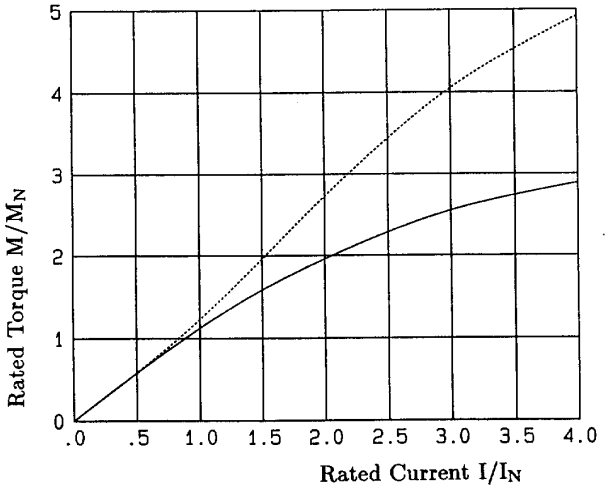

Fig. 3: Asymmetrical rotor with outside iron pieces. Rated torque as a function of the rated current. $\psi = -30°$: — measurement, - - 2D field calculation, M_N=4Nm.

With a 2D-finite Element package the torque of this motor was calculated by virtual displacement [2] with an load angle of $\psi = -30°$ as a function of the current Fig. 3. The comparison of calculation and measurement shows a wide difference. The torque reduces quite enormously at high current levels. A measurement of a symmetrical rotor design with the same e.m.f. delivers simular results. There seems to be no difference for short rotor length whether using a symmetrical or an asymmetrical rotor, nearly no additional torque contribution can be recieved. This effect will now be investigated. Due to the saturation effect a finite element package is used. The numerical field calculation in 3D will be compared with 2D to explain this effect.

IV. Field Calculation with Finite Elements

The finite element field calculation was done with the finite element package MAGNET of Infolytica. A rotor with buried magnets Fig.5 and the salient pole rotor Fig. 4 with two outside magnet pieces was investigated. The motor has a number of pole pairs of p=3, a slot number of q=2 and a three phase stator winding.

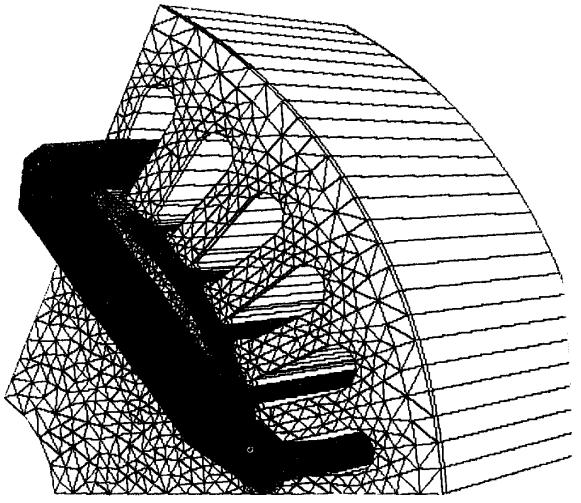

Fig. 4: 3D Motor with the salient pole rotor.

Rated torque of both motors is 13 Nm, rated speed 3000 rpm. The optimal load angle ψ was estimated in 2D with a numerical interpolation of DSC [3]. The influence of the laminated rotorsheets in 3D is neglegted in the field calculation, but will be taken later into consideration. The torque output for different current levels is calculated with the virtual displacement method of elements [2], which will be compared with a flux method in 2D. This flux method will be used to estimate the torque of the 3D field calculation, because the finite element package delivers slices with the flux density vector. An excess of the scalar potential is not existent. This flux method used has been proved by measurements and investigations have shown that it is very independent of the discetisation of the model due to the virtual displacement method.

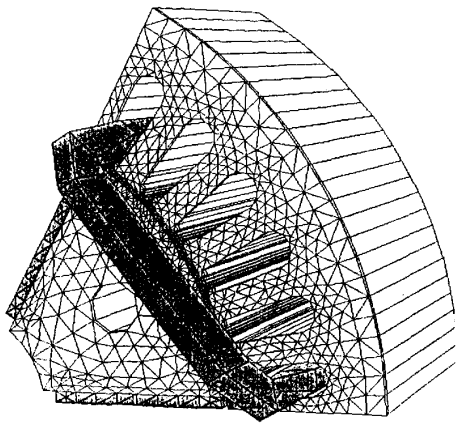

Fig. 5: 3D Motor with radial magnets and with one coil.

A. Torque Calculation

The maxwell stress tensor is dependend on the discretisation of the model and delivers too inaccurate results. The virtual displacement method [2] for the torque calculation can easily be applied in 2D, if the vector potential for each displaced node is known. With the 3D-package of MAGNET just slices can be done to get the flux density, which then can be processed. To achieve a comparable method for the torque calculation in 3D, the flux in one winding will be estimated by:

$$\Psi_{coil} = w_{coil} \int_{coil} \vec{B} d\vec{A} \quad . \tag{4}$$

With respect to the stray flux of the slots, the average flux of three different layers in one coil is calculated.

For 2D field calculation the flux can be estimated with the vector potential:

$$\Psi_{coil} = w_{coil} \oint_{coil} \vec{A} d\vec{s} = l_i \cdot (A_{slot1} - A_{slot6}) \quad . \tag{5}$$

The vector potential of the slot is approximated as follows:

$$A_{slot} = \frac{1}{F_{slot}} \sum_{i}^{N} A_i i \cdot F_i \quad . \tag{6}$$

F_{slot}	:	Area of the slot
A_i	:	Vector potential at the middle of the element i
F_i	:	Area of the element i
l_i	:	motor length
w_{coil}	:	Number of winding of the stator coil
N	:	Number of elements in the slot

The effect of the chored winding of $\frac{s}{\tau_p} = 5/6$ on the induced voltage then can easily be taken into account by addition of the flux of the two coil layers. With this motor the flux can be estimated for six rotor positions by one pole pitch. The derivative with a DFT gives the induced voltage $U_i(t)$:

$$U_i(t) = RI(t) + \frac{\psi}{dt} \quad . \tag{7}$$

The resistance will be neglected (R=0). The influence of the rotor sheets on the induced voltage will be taken into account with a factor of $l_{Fe} = 0.96 \cdot l_i$. Now also skewed slots can be taken in consideration [4]:

$$U_i(n) = \sum_{k=0}^{N} B_k \cos(2\pi \frac{nk}{2N} - \phi_k) \quad , \tag{8}$$

$$U_i(n)_{skewed} = \sum_{k=0}^{N} B_k \chi_k \cos(2\pi \frac{nk}{2N} - \phi_k) \quad , \tag{9}$$

$$\chi_k = \frac{\sin(k\frac{\pi}{6q})}{k\frac{\pi}{6q}} \quad . \tag{10}$$

n	:	n.th position
N	:	Number of positions for one pole pitch

If the speed n of the rotor is constant, the torque M and the Power P can be calculated with the three phases u, v, w as follows:

$$P(t) = \sum_{k}^{u,v,w} U_{ik}(t) \cdot I_k(t) \quad , \tag{11}$$

$$M = \frac{P(t)}{2\pi n} \quad . \tag{12}$$

A comparision of this method to the virtual displacement method delivers very good results, which are improved by measurements.

B. Calculation of the Reactances

For the estimation of the reactances the amplitude $\hat{U}$(I) and phase ϕ(I) of the fundamental wave of the induced voltage U_i at load and noload are calculated. The load angle ψ of the current is known and the reactances of the quadrature and direct axis can be calculated as follows:

$$X_q = \frac{\hat{U}_i(0)\sin(\phi(0) - \phi(I_N))}{\sqrt{2} I_N \cdot \cos(\psi)} \quad , \tag{13}$$

$$X_d = \frac{(\hat{U}_i(0)\cos(\phi(0) - \phi(I_N)) - \hat{U}_i(0))}{\sqrt{2} I_N \cdot \sin(\psi)} \quad . \tag{14}$$

V. Results and Conclusion

The motor in Fig. 5 is calculated at different current levels and with different rotor lengths. The maximum distance of the stator coils outside the slots is 25 mm. The motor has a diameter of 135 mm. Different rotor lengths

to stator lengths are also taken into consideration. The slots are not skewed and six rotor positions are taken into account. The results of the 3D field calculation are shown in Table I and Table III and the comparable results for 2D are given in Table II and IV. The shorter the rotor, the less the torque per length and X_q/X_d decreases (see also Fig. 6 and 7). The main reason for both rotor designs is the synchronous torque. The shorter the rotor the more the stray flux raises. In both cases the reluctance torque contribution decreases (Fig. 6). But the negative direct current component has still an influence on the dynamic behaviour (Fig. 7). For the vertical rotor design the end winding leakage has a very bad influence on the reluctance torque. Here magnet material can be saved, if the rotor length is choosen smaller than the stator. The oposite case is not very effective for the output torque and requires more magnet material. If less magnet material is used, the induced voltage is also smaller, therefore in Table I and III the rated torque m_{3D}/m_{2D} is calculated due to the rotor length. The results show that for short rotor designs the salient pole rotor is more effective. The torque reduces not as much as for the vertical rotor design.

TABLE I
RESULTS OF 3D CALCULATION OF VERT

rotor $[mm]$	stator $[mm]$	X_q/X_d	M/M_N (3D)	m_{3D}/m_{2D}	I/I_N
17	17	1.29	1	0.86	1
17	17	1.15	1.92	0.84	2
17	17	1.04	2.19	0.77	3
95	95	1.45	1	0.97	1
95	95	1.27	2.02	0.95	2
95	95	1.14	2.78	0.94	3
21	17	1.23	1	0.79	1
13	17	1.35	1	0.91	1
13	17	1.23	2.04	0.94	2
13	17	1.11	2.72	0.90	3

TABLE II
RESULTS OF 2D CALCULATION OF VERT

X_q/X_d	M/M_N	I/I_N
1.49	1	1
1.31	2.11	2
1.25	2.88	3

TABLE III
RESULTS OF 3D CALCULATION OF M57

rotor $[mm]$	stator $[mm]$	X_q/X_d	M/M_N (3D)	m_{3D}/m_{2D}	I/I_N
17	17	1.46	1	0.96	1
17	17	1.33	2.06	0.94	2
17	17	1.20	2.89	0.88	3
95	95	1.79	1	0.98	1
95	95	1.63	2.136	0.99	2
95	95	1.47	3.190	0.99	3

TABLE IV
RESULTS OF 2D CALCULATION OF M57

X_q/X_d	M/M_N	I/I_N
1.69	1	1
1.59	2.121	2
1.46	3.166	3

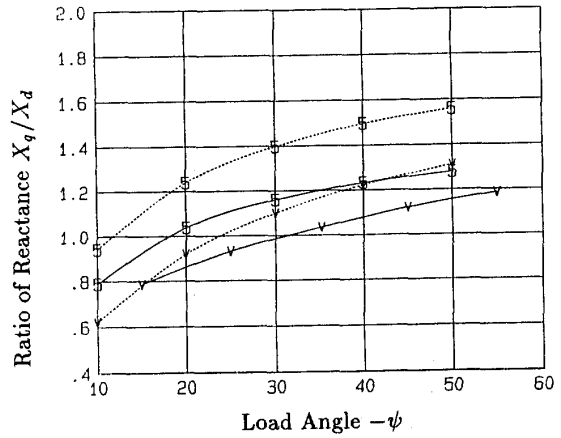

Fig. 6: Ratio of reactance dependent of the load angle ψ at 3 I_N: — 17 mm (3D), - - (2D), V: VERT, 5: M57

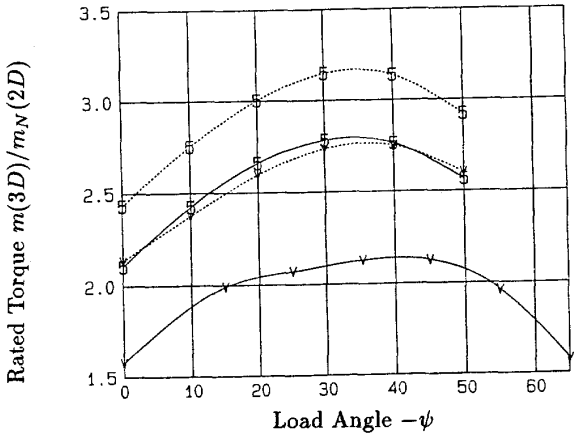

Fig. 7: Rated torque dependent of the load angle ψ at 3 I_N: — 17 mm (3D), - - (2D), V: VERT, 5: M57

REFERENCES

[1] G. Henneberger,"Dynamic Behaviour and Current Control Method of Brushless DC-Motors with Different Rotor Designs", 3rd European conference on power electronics and applications, vol.3, p. 1531-1536, October 1989, Aachen, Germany

[2] J.L. Coulomb, G. Meunier, "Finite Element Implementation of Virtual Work Principle for Magnetic or Electric Force and Torque Computation", IEEE Trans. on Magnetics Vol. MAG-20 No 5., Sept 1984

[3] Himmelblau, D.M., *Applied nonlinear Programming*, Mc. Graw-Hill, 1972

[4] Richter, Rudolf, *Elektrische Machinen*, p.123, 1954